Vibrational and dielectric properties of monolayer transition metal dichalcogenides

Nicholas A. Pike,[1,2,*] Antoine Dewandre,[2] Benoit Van Troeye,[3] Xavier Gonze,[4] and Matthieu J. Verstraete[2]

[1]*Centre for Materials and Nanotechnology, University of Oslo, NO-0349 Oslo, Norway*

[2]*Nanomat/Q-Mat/CESAM, Université de Liège and European Theoretical Spectroscopy Facility, B-4000 Liège, Belgium*

[3]*Université Catholique de Louvain, Institute of Condensed Matter and Nanosciences (IMCN) and European Theoretical Spectroscopy Facility, B-1348 Louvain-la-Neuve, Belgium*

[4]*Université Catholique de Louvain, Institute of Condensed Matter and Nanosciences (IMCN) and European Theoretical Spectroscopy Facility, B-1348 Louvain-la-Neuve, Belgium and Skolkovo Institute of Science and Technology, Moscow, Russia*

(Received 25 March 2019; revised manuscript received 13 June 2019; published 29 July 2019)

First-principles studies of two-dimensional transition metal dichalcogenides have contributed considerably to the understanding of their dielectric, optical, elastic, and vibrational properties. The majority of works to date focus on a single material or physical property. Here we use a single first-principles methodology on the whole family of systems to investigate in depth the relationships between different physical properties, the underlying symmetry, and the composition of these materials, and observe trends. We compare to bulk counterparts to show strong interlayer effects in triclinic compounds, and relationships between these monolayer compounds become apparent. These trends can then be exploited by the materials science, nanoscience, and chemistry communities to better design devices and heterostructures for specific functionalities.

DOI: 10.1103/PhysRevMaterials.3.074009

I. INTRODUCTION

Since the discovery of graphene [1], the search for useful two-dimensional materials [2–4] as components of more complex electronic [5–8] or electro-optical devices [9,10] has expanded significantly. Many two-dimensional materials display unique properties, and one can combine the individual layers [11–15] as building blocks to produce increasingly complex devices [16,17]. Recent studies have demonstrated the power of density functional theory (DFT) [18] in identifying novel two-dimensional materials that have useful electronic and optical properties [19–22] and of density functional perturbation theory (DFPT) in determining the stability and vibrational properties of these materials [23,24].

There is a significant amount of work, both experimental [25–31] and theoretical [32–37], focusing on how the properties of transition metal dichalcogenide (TMD) monolayers differ from their bulk counterparts. However, even with this copious amount of experimental and theoretical work, a wide-ranging analysis of the vibrational and dielectric properties of the monolayer compounds, and a systematic comparison of these properties with their bulk counterparts, has received little attention. Such an analysis is essential to understand and appreciate the unique properties that the monolayers and their bulk counterparts have.

In these layered materials, the interlayer interaction is generally weak compared to the intralayer one [38,39]. Consequently, one expects the intrinsic chemistry of the constituent layers to remain relatively unaffected by stacking. To some extent, the physical properties of the bulk or van der Waals (vdW) heterostructures should be related to the properties of the individual layers. Failures of this approximation include the recent discovery of superconductivity in *bilayer* graphene twisted at a specific angle [40], superconductivity in bilayer graphene/h-BN layers [41], and the ultralow thermal conductivity in disordered, layered WSe_2 [42]. Additionally, when vdW layers are stacked during device construction, one or both of the lattices may compensate by expanding or contracting, to maximize the interlayer interactions at the expense of elastic energies [43]. This can result in the formation of a Moiré pattern and possible associated modification of electronic properties [16,44–48], as observed, for example, in the MoS_2-WSe_2 vdW heterostructure [49]. Knowledge of the structural properties of the monolayers leads to better device construction and orientation by taking into account the nature of each material (e.g., elasticity, dielectric response).

The theoretically predicted vibrational properties can easily be compared to Raman and infrared spectroscopy experiments [50,51] in order to identify the number of layers, strain states, and certain defect states. The related dielectric properties are critical as they relate directly to the electro-optical properties of these materials. With this in mind, we investigate systematically the physical, electrical, dielectric, and optical properties for the most common and stable TMD monolayers. These include the in-plane lattice parameters, the thickness of an individual layer, electronic energy gap, binding energy, and the elastic, dielectric, Born effective charge, piezoelectric, and nonlinear optical tensors.

In this article, we focus on the most common and stable TMDs, which cover the following three different symmetry classes: hexagonal (h)-TMDs (MoS_2, $MoSe_2$, $MoTe_2$, WS_2, and WSe_2), trigonal (t)-TMDs (TiS_2, $TiSe_2$, $TiTe_2$, ZrS_2, and $ZrSe_2$), and triclinic (tc)-TMDs (ReS_2, $ReSe_2$, and TcS_2). This allows us to determine the effects of chemical composition and the local environment. We find both expected trends

*nicholas.pike@smn.uio.no

and unexpected ones in the elastic, dielectric, and vibrational properties. In particular, Young's modulus for the triclinic compounds increases as the lattice parameter increases, which is counter to the intuition suggested in Ref. [52] linked to bond strength and charge transfer. Furthermore, some of these compounds have a bending rigidity that is 2–3 times larger than graphene, and even more so in MoS_2, which had previously led the community to believe that TMDs were unadapted to flexible electronics. In the main text below, a single sulfide member from each structural family is given as an example alongside the aggregate trends. Details on the remaining materials can be found in the Supplemental Material (SM) [53].

II. CALCULATION METHODS

To determine the properties of our chosen materials, DFT [18,54] and DFPT [55–57] calculations are undertaken using the ABINIT software package [58–60]. Consideration of the usual DFT approximations (pseudopotential, exchange correlation, dispersion correction, and spin-orbit coupling) is summarized in Ref. [61] for the bulk counterparts of these systems, and are systematically checked during our investigations of the monolayers.

For our calculations, we have used the generalized gradient approximation Perdew-Burke-Ernzerhof (GGA-PBE) exchange-correlation functional and Trouiller-Martins pseudopotentials [18,62,63], generated with the FHI98PP code for all elements except W and Ti. In the case of W, we exploit a pseudopotential generated with the OPIUM code [64], which produces accurate relaxed lattice parameters, while for Ti, we use an ONCVPSP [65] generated pseudopotential, which correctly reproduces the Kohn anomalies in the corresponding materials. Long-range dispersion forces are included using Grimme's DFT-D3 scheme [66], as implemented in ABINIT, for both the ground-state and response-function parts of the code [67,68]. All electronic and response-function computations use the relaxed geometries. The residuals for the ground-state and first-order wave function were converged below 10^{-18} and 10^{-10}, respectively. We perform convergence studies of the energy cutoff and the reciprocal-space k sampling using a Monkhorst-Pack grid [69] such that the total-energy change was less than 0.01 meV per unit cell. These studies provide a range of energy cutoffs between 20 and 50 Ha, depending on the atomic species, as outlined in the SM [53], and a k-point mesh of $8 \times 8 \times 1$ was used for all stages of the calculation. During structural relaxation, we use the Broyden-Fletcher-Goldfarb-Shanno minimization procedure [59] to relax the positions and unit cell simultaneously, with a maximum force below 1.0×10^{-7} Ha/Bohr. For all the calculations presented in the main text, spin-orbit coupling was not included. We have found it makes little to no difference in the calculated lattice parameters and vibrational properties of similar bulk TMD materials [61]. However, spin-orbit coupling does have an influence on the allowed optical transition in monolayer materials, which we discuss below.

Our calculated Raman spectra and nonlinear optical tensor [70] use the local density approximation (LDA) exchange correlation [71] for the calculation of the third derivative of the exchange-correlation part of the energy. We have rescaled the Raman intensities by their maximum value: usually experiments do not report absolute values and only relative differences in intensity are comparable. In each case, we plot the Raman frequencies assuming a fixed Lorentz broadening for the spectral lines of 1.0×10^{-5} Ha and a laser wavelength of 532 nm, a typical frequency used in Raman experiments [72,73]. Our plotted Raman data include in-plane (XX and YY), out-of-plane (ZZ), and powder-averaged spectra, which are calculated assuming a random orientation of monolayer flakes, similar to what is done in Ref. [74].

III. RESULTS AND DISCUSSION

All TMDs consist of a layer of metal atoms packed between two layers of chalcogen atoms. The monolayer h-TMDs show sixfold octahedral coordination (in the form of a trigonal prism) in the layer and space group $P\bar{6}m2$. In Fig. 1(a), we show a typical h-TMD layer in the xy and xz planes containing three atoms per unit cell. The t-TMDs consist of chalcogen atoms forming a trigonal antiprism, with space group $P\bar{3}m1$, as shown in Fig. 1(b) where there are two chalcogens and one transition metal atom per unit cell. Finally, in Fig. 1(c), we show a typical tc-TMD composed of 12 atoms, grouped into two types of inequivalent distorted octahedra, and $P\bar{1}$

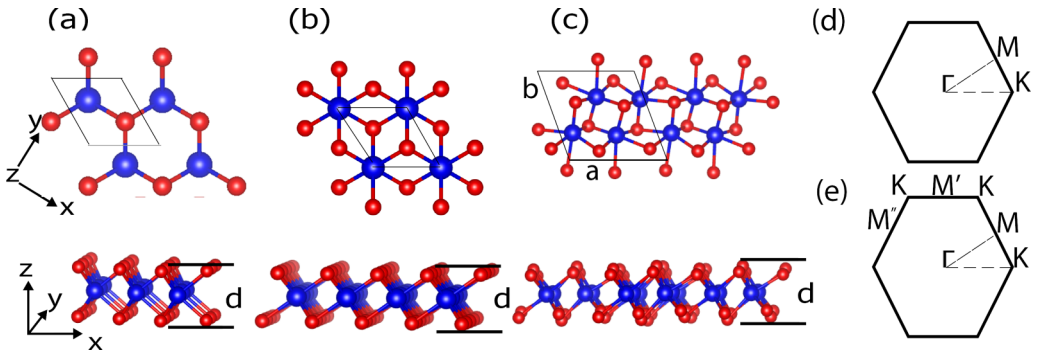

FIG. 1. Sketch of a generic monolayer (a) h-TMD, (b) t-TMD, and (c) tc-TMD where the transition metal is given in blue and the chalcogen atoms are in red. (d) The Brillouin zone for the h and t compounds in two dimensions and (e) the Brillouin zone for the tc compounds in two dimensions. The two-dimensional unit cells for each compound are outlined with gray boxes and the a and b lattice parameters of the tc compounds are indicated in (c).

TABLE I. Properties of monolayer MoS_2, ZrS_2, and ReS_2 with our calculations in the first subcolumn, literature values in the second, and the reference in the third. We report the in-plane lattice parameters, a, and b, the geometric thickness of an individual layer, d, the in-plane components of the elastic tensor per unit area (c_{ij}), Young's modulus (E_i), Poisson's ratio (ν_{ij}), bending rigidity (κ_i), Kohn-Sham electronic band-gap energy (E_g,) binding energy (E_b), in-plane components of the dielectric tensor (ϵ^0_{ij}), optical dielectric tensor (ϵ^∞_{ij}), and Born effective charges (Z^*_{ii}) on the transition metal atom (blue in Fig. 1), piezoelectric coefficient (e_{11}), nonlinear optical coefficient (d_{16}), Debye temperature (θ_D), average speed of sound (v_{avg}), and the Helmholtz free energy at zero temperature [$\Delta F(0)$]. * indicates the predicted gap is indirect, † indicates the values are divided by 2 for the sake of comparison with other TMDs, f.u. = formula unit, and values in brackets correspond to other first-principles calculations. For the tc compounds, the two lines of the Born effective charge tensor correspond to the two inequivalent transition metal atoms.

	MoS_2			ZrS_2			ReS_2		
	Calc.	Lit.	Ref.	Calc.	Lit.	Ref.	Calc.	Lit.	Ref.
a (Å)	3.165	3.200 [3.19]	[19,75]	3.695	[3.68, 3.67]	[19,37]	6.414	[6.407]	[21]
b (Å)							6.581	[6.515]	[21]
d (Å)	3.186	3.172	[75]	2.967	3.625†	[76]	3.541	3.50†	[29]
E_g (eV)	1.896	1.85 [1.6]	[11]	1.449*	[1.02*,1.2*]	[19,35]	1.442*	[1.85*]	[77]
E_b (meV/Å^2)	30.316	[21.6;28.8]	[19]	19.043	[19.0;24.1]	[19]	1.010		
c_{11} (Ha/Bohr^2)	0.082	[0.081]	[21]	0.042	[0.046]	[21]	0.106	[0.092]	[21]
c_{22} (Ha/Bohr^2)							0.108	[0.092]	[21]
c_{12} (Ha/Bohr^2)	0.018	[0.020]	[21]	0.006	[0.008]	[21]	0.019	[0.018]	[21]
c_{66} (Ha/Bohr^2)	0.032	[0.03]	[21]	0.018	[0.019]	[21]	0.004		
E_x (Ha/Bohr^2)	0.078	0.11 [0.076]	[21,78]	0.041	[0.044]	[21]	0.102	[0.088]	[21]
E_y (Ha/Bohr^2)							0.104	[0.089]	[21]
ν_{xy}	0.218	[0.25]	[79]	0.14	[0.18]	[21]	0.182	0.207 [0.19]	[21,80]
κ_x (eV)	10.96	9.93	[81]	5.17			3.09		
ϵ^0_{xx}	20.20			43.35			23.28		
ϵ^0_{yy}							20.85		
ϵ^0_{xy}							0.15		
ϵ^∞_{xx}	19.98			14.48			18.72		
ϵ^∞_{yy}							20.65		
ϵ^∞_{xy}							0.25		
Z^*_{xx} (e)	−1.088	[−1.004]	[82]	6.205			−1.496		
							−0.532		
Z^*_{yy} (e)							−0.556		
							0.296		
e_{11} ($\times 10^{-10}$C/m)	2.77	2.9	[83]						
d_{16} (Å^2/V)	0.406	1.0	[84]						
θ_D (K)	177.48			133.08			86.72		
v_{avg} (km/s)	4.068			3.269	[3.4]	[36]	3.213		
$\Delta F(0)$(kJ/mol)	14.567			10.962			46.093		

space-group symmetry. Several authors [77,85,86] have noted that the two-dimensional Brillouin zone of these materials is similar to the in-plane Brillouin zone of a hexagonal or trigonal system, as shown in Fig. 1(e). There are inequivalent M points on the faces of the Brillouin zone due to the difference in lattice vector lengths. In the band structures and Raman spectra that follow for the tc compounds, we plot only the path Γ-M-K-Γ, where M corresponds to ($\frac{1}{2}$,0,0), the a axes of the h, t, and tc compounds have been aligned, and we use a 120 degree unit cell for h and t systems.

The accurate calculation of monolayer properties with periodic boundary conditions requires a large vacuum to separate the periodic images. To compare the material properties which depend on volume, such as the dielectric tensor, to their bulk counterparts, the unit-cell volume must be rescaled. Similarly, the reduced dimensionality of the system means that the phonon band structures, and corresponding density of states, have different frequency dependencies in two and three dimensions. This dimensionality manifests itself in a distinct quadratic acoustic mode in the phonon band structure and as an apparent logarithmic divergence in the thermal properties of the system. In reality, the divergences of the thermal properties are suppressed by this quadratic ZA mode, which plays a dual role as a significant source of occupied phonon states and as a scattering source, as shown for graphene [87,88]. We do not present thermal properties here as our calculations stay at the harmonic level in ABINIT.

In Table I and Figs. 2(a) and 2(b), we show our calculated in-plane lattice parameters with the corresponding available literature data [37,75,89–95]. The lattice parameters should

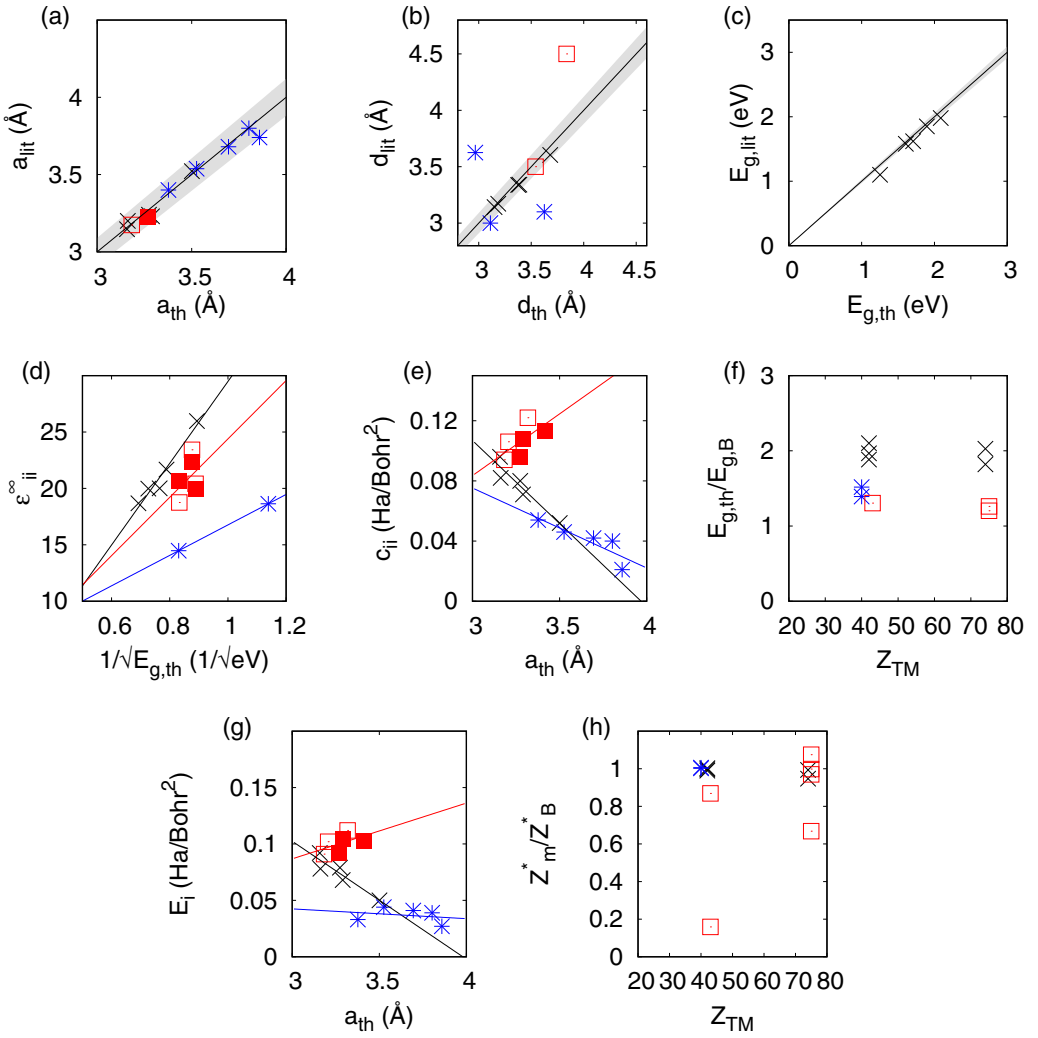

FIG. 2. Comparison between our theoretical values (th) and literature values (lit) for the principal dielectric and structural properties of TMDs. h-TMDs are shown as black crosses, t-TMDs as blue stars, and tc-TMDs as red squares (xx component as empty and yy component as solid squares). (a) The in-plane lattice parameter, (b) thickness of the monolayer, and (c) a comparison between the electronic band-gap energy $E_{g,th}$ and the optical band-gap energy for the h-TMDs. The solid gray wedge in (a)–(c) represents $\pm 3\%$ error. (d) The relationship between the dielectric response and the inverse square root of the calculated electronic energy gap, with the solid line indicating a linear fit of the semiconducting TMDs for each family. (e) The relationship between the in-plane elastic constants and the in-plane lattice parameters. (f) and (h) compare monolayers with bulk, for calculated band-gap energies and Born effective charges with the atomic number of the transition metal (Z_{TM}) on the horizontal axis. (g) The calculated Young's modulus vs lattice parameter. In (a), (e) and (g), the lattice parameter of the tc compounds is divided by two for the sake of comparison with other TMDs.

be compared to their bulk counterparts (MoS_2: 3.162 Å; ZrS_2: 3.687 Å; ReS_2: 6.420 and 6.587 Å) [61] and show only slight changes (0.2%) of the in-plane lattice parameters in Fig. 2(f). For the tc compounds, the calculated angle between the a and b lattice vectors is 60.2 degrees. The thickness of an individual layer, d, defined here as the vertical distance between the outermost chalcogen atoms, compares favorably to experimental data on freestanding layers for the h compounds and gives a reasonable comparison to half the experimentally measured thickness in measurements of monolayers on substrates [29,76,96–98]. Note that the observed differences between our calculated thickness and half the experimental thickness are most likely due to the changing interaction between the monolayer and substrate.

The binding energy E_b of a given TMD material is defined as the gain of energy resulting from the stacking of the corresponding TMD monolayers on top of each other in the optimal stacking sequence. In other words, E_b represents the difference in energy between the total energy of the bulk TMD compound ($E_{T,\text{bulk}}$) and the number of layers per primitive cell (n) times the total energy of a monolayer ($E_{T,\text{mono}}$) as

$$E_b = E_{T,\text{bulk}} - nE_{T,\text{mono}}. \quad (1)$$

While most of the binding energies for these TMD monolayers lie between 20 and 40 meV/Å^2, which is consistent with Ref. [19], the tc-TMD compounds have binding energies of the order of only 1 meV/Å^2. This small value is consistent with experimental Raman measurements and DFT interfacial

interaction energies, indicating that the interlayer coupling in the tc compounds is relatively weak [29,30,99]. In Raman measurements, there is only a very small shift in the peak frequencies between the monolayer and the bulk, and the ZO optical mode in tc bulk is lower than in MoS_2 [29].

The planar elastic constants (per unit area; see Table I) are comparable to their bulk counterparts when rescaled to account for the vacuum spacing. In two dimensions, the only nonzero components of the elastic tensor are c_{11}, c_{12}, c_{22}, and c_{66} [$c_{66} = (c_{11} - c_{12})/2$ for the hexagonal and trigonal systems] [100,101]. A direct comparison between these elastic tensor components and their bulk values reveals almost no difference, as is often assumed in finite-element analysis [102]. Our DFT calculations are an important sanity check for the whole set of common TMDs.

To compare to experiment, we calculate several derived properties, such as Young's modulus and Poisson's ratio, taking into account the two-dimensional nature of the system, as shown in the SM [53,100,103]. Our calculated Young's modulus agrees well with experimental measurements on freestanding monolayers [78,104].

Of particular interest is the relationship between our calculated in-plane lattice constant and the components of the elastic tensor for each symmetry class of compounds. As shown in Fig. 2(e), there exists a roughly linear relationship between the in-plane lattice parameter and c_{11} over the range of compositions and chemistries. Reference [52] suggests that the decrease in Young's modulus of these materials is correlated to the increase in the lattice parameter and a decrease in charge transfer. The hypothesis is that by increasing the lattice parameter of a material, one would decrease the atomic overlap of the orbitals and thus decrease the electronic interaction, which would in turn soften the material and lower the Young modulus. We have plotted this first relationship in Fig. 2(g) and demonstrate that the relationship with lattice parameter holds for the h- and t-TMDs, but not for the tc-TMDs. The Born effective charge quantifies the charge transfer and polarizability in these monolayer systems; a comparison to their bulk counterparts is given in Fig. 2(h) where the ratio of the monolayer to the bulk Z^* of Ref. [61] is given. Figure 2(h) reveals no difference in these systems for the h and t compounds, but does show a strong scatter in the Born effective charge in the tc compounds: isolating a monolayer rearranges the charge and polarizability of the inequivalent octahedra. As a measure of the static charge rearrangement, we present the Bader charges of the tc compounds compared to their bulk values and compare these with the bulk and monolayer Bader charges of MoS_2 in the SM [53]. We find that the Bader charge also differs between the monolayer and the bulk for the triclinic compounds, but there is no such difference for MoS_2. In summary, the tc compounds rearrange charges more in their monolayer forms.

It was recently demonstrated [68,105] that the bending modes are of critical importance to our understanding of Moiré patterns in vdW heterostructures. We calculate the bending rigidity κ using Kirchhoff-Love theory for thin plates [106] as

$$\kappa = \frac{Ed^3}{12(1-\nu^2)}, \tag{2}$$

where d is the thickness of the individual layer with Young's modulus in GPa. As noted in Refs. [107,108], the definition of the thickness d of the thin plate is potentially ambiguous when dealing with two-dimensional materials. Experimentally, the thickness of these materials frequently includes the height of the vdW gap. However, as we calculate freestanding monolayers, there is no vdW gap and we define the thickness as the vertical distance between the outermost atoms. This value is easily calculated in DFT and compares well to measurements of freestanding layers [81]. With this definition of the thickness, we agree well with the theoretical calculations of the bending rigidity of Lai *et al.* [107]. We calculate the bending rigidity using the larger of the two in-plane Young's moduli and the maximum thickness of the layer, as reported in Table I. The bending rigidity of these compounds is significantly greater than for graphene ($\kappa = 1.2$ eV [109]), with the notable exception of the tc-TMDs: with their increased internal degrees of freedom and different sizes of octahedra, the materials are just two to three times stiffer than graphene, making them two to three times softer than MoS_2, and potential candidates for flexible optoelectronics.

The piezoelectric tensor can be nonzero, due to the lack of inversion symmetry, for the h compounds. Our calculations provide a distinct nonzero component of the piezoelectric tensor which can be compared to Zhu *et al.* [83] and other theoretical results [110], after taking into account the vacuum spacing.

The calculated Kohn-Sham electron band structures for our compounds are given in Fig. 3 without the inclusion of spin-orbit coupling. Monolayer h-TMDs display both direct

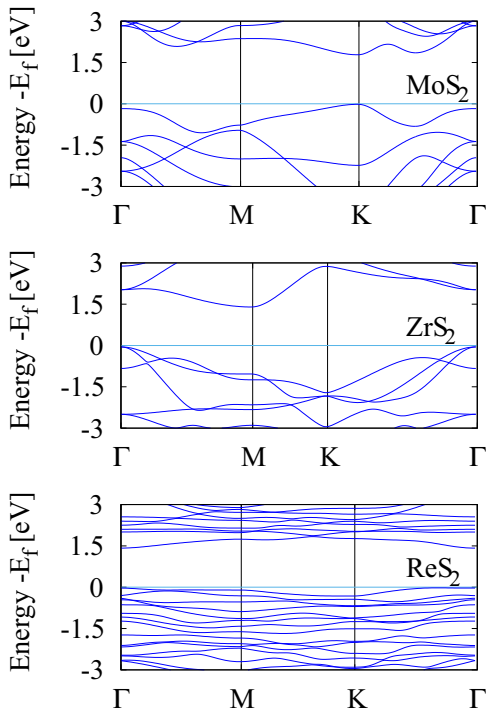

FIG. 3. Calculated Kohn-Sham band structure for the three example materials with the Fermi energy shifted to the zero of energy. The band structure is plotted along a path of high symmetry in reciprocal space.

and indirect electronic band gaps, agreeing with earlier work [28,113], and which depend strongly on the residual strain in the system.

The electronic band gaps are given in Table I and denoted with a star when they are indirect. We compare our calculated electronic band gaps with the measured optical band-gap energy [11,28,77,114,115]. Although DFT normally underestimates the (quasiparticle) band gap of bulk materials, for the h-TMDs we find an average difference of only 6% compared to experimental optical gaps [116–120]. We compare electronic band-gap energies calculated without spin orbit to optical band-gap energies in Fig. 2(c) for the hexagonal TMD. It is now well established (e.g., in Ref. [121]) that there are strong excitonic effects in TMD monolayers, with a large two-dimensional (2D) binding energy which shrinks the optical gap: this approximately counterbalances the intrinsic DFT Kohn-Sham band-gap error [122,123]. The effects of spin-orbit coupling on the band structure are large ($\approx$100 meV at K in monolayer TMDs) [124] (as shown in the SM [53] for a single compound), but mainly splits off the second valence band, with little effect on the value of the band gap. Another important factor for the TMDs [124] is the optical spin-selection rules: the allowed transition must conserve spin and goes from the top valence band to the first or second conduction band, a further difference in the optical gap of $\approx$30 meV (much smaller than the valence band). The conduction-band minima at K and Λ (located between K and Γ, often also called Q) are nearly degenerate in our TMD band structures, which indicates very low residual strain [27,125].

Our calculations indicate that some of the t-TMDs are metallic, while the tc-TMDs are all semiconducting. The opening of the electronic band gap when compared to the bulk is given in Fig. 2(f), showing the ratio of the calculated electronic band gap of the monolayer, $E_{g,m}$, to that for the bulk, $E_{g,B}$ (from Ref. [61]) regardless of whether the band gaps are direct or indirect. For all the nonmetallic materials, we find an opening of the electronic band gap. For the hexagonal materials, this is approximately a doubling compared to their bulk counterparts and agrees with recent work indicating that as the number of layers decreases, the nature of the dielectric environment can change considerably (e.g., Ref. [126]).

To compare our calculated dielectric tensors to their bulk counterparts, we must once again take into account the vacuum spacing. A comparison between ϵ^{∞} and the inverse square root of our calculated band-gap energy in Fig. 2(d) shows the expected linear dependence of these two quantities [127] with different proportionality constants for each symmetry class. The magnitude of the Born effective charge tensor in these materials can be experimentally measured in infrared reflectivity experiments. The sign of the Born effective charge and its origin are discussed extensively in Ref. [128] and are counterintuitive for the h- and tc-TMDs. The Born effective charges calculated here agree with previous DFT and DFPT calculations [82,129,130] and with their bulk counterparts, as

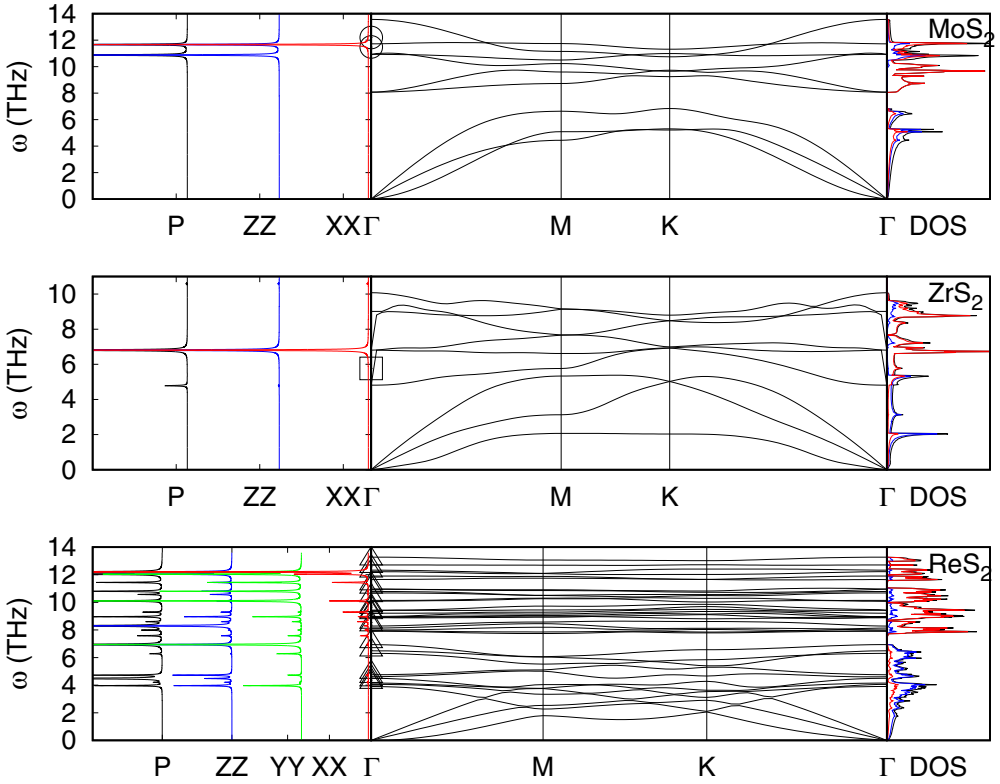

FIG. 4. Raman spectra, phonon band structure, and phonon density of states of the example materials. Experimental data from Refs. [30,31,111] are shown as points at Γ. The high-symmetry path in reciprocal space is from Ref. [112]. For the Raman spectra, red lines correspond to XX polarization, green lines to YY polarization, and blue lines to ZZ polarization. The black Raman spectra correspond to a powder spectra. In the density of states plots, the blue line corresponds to the density of states of the transition metal atom, the red line corresponds to the chalcogen atom, and the black line corresponds to the total density of states.

shown in Fig. 2(h). While no significant changes are observed for the h and t compounds, the magnitude (and sign for TcS_2) of the Born effective charge changes for the tc compounds due to differences in the charge and polarizability between the monolayer and the bulk.

We compare our nonlinear optical tensor to experimental work [84,131] after rescaling to account for the vacuum spacing, as was done in Ref. [132]. Comparisons to other literature results require care, as our calculated values are the zero-frequency limit of the frequency-dependent nonlinear susceptibility. With this in mind, we find an agreement with the order of magnitude of experimental measurements [132,133]. Our calculations indicate that the nonlinear susceptibilities of the h compounds change sign when going from S to Se to Te. The overall size of the tensor element decreases as the calculated band gap decreases, as was shown in other work [132].

The thermal and acoustic properties of our compounds come from calculations of the interatomic force constants including the dispersion correction [61]. Our calculated phonon band structures, phonon density of states, and Raman spectra for the model compounds are shown in Fig. 4, with experimental Raman frequencies at Γ from Refs. [11,28,30,72,90,111,115,134]. Here, the phonon density of states contributed by the transition metal atoms is given in blue and the chalcogen atoms in red. The nearly quadratic behavior near $q \rightarrow 0$ indicates (Ref. [135]) that there is no internal strain within these materials after relaxation. The ZA mode is not purely quadratic as the rotational sum rule is not imposed explicitly in our calculations. We have investigated the effects of an increased q-mesh density on this ZA mode and are using a q mesh such that the frequencies of the ZA mode near $q \rightarrow 0$ are converged to better than 0.1%. Additionally, as reported in Refs. [136,137], we find the longitudinal optical (LO) and transverse optical (TO) modes are strongly affected by the dielectric environment of the two-dimensional layer for q points near Γ. Our phonon band structures use the standard 3D Coulomb correction, and the LO-TO splitting is unrepresentative of a truly 2D system (Ref. [136]). Our calculations of the Born effective charges compare well to other theoretical work [82].

In some of these compounds, our phonon band structures show Kohn anomalies due to their small or zero band gaps [138–141]. When compared to their bulk counterparts [61], the Kohn anomalies appear at M for both bulk and monolayer TiS_2 and $TiSe_2$, whereas in the case of bulk $TiTe_2$, we find no Kohn anomaly at M in the bulk but do find the Kohn anomaly at M in the monolayer. This agrees with the fact that a charge density wave transition is not observed in bulk $TiTe_2$, whereas one was observed in the monolayer [25]. Our calculations agree with other theory work [142] indicating that the relative size of the Kohn anomaly is a strong function of the smearing used during the DFPT calculation. Here, a smearing of 10 K is used. Additionally, for the tc compounds, our calculated phonon band structures show that they are stable at Γ, which is consistent with the theoretical predictions in Ref. [73], and are Raman active [29,30,73,134].

IV. CONCLUSIONS

With distinctive crystal symmetries and dimensional effects, the transition metal dichalcogenides display a variety of properties that can be exploited for future optoelectronic device applications. Our first-principles calculations of the monolayer TMDs reveal both significant similarities and differences between monolayer and bulk compounds, in terms of their electronic and vibrational properties. These are crucial when modeling the elastic/mechanical and dielectric properties of these materials.

The dimensionality of the monolayer systems brings about changes to many of the physical and electric properties. The most noticeable changes occur due to the switch from an indirect to a direct electronic band gap and, to a lesser extent, the appearance of finite nonlinear optical coefficients and piezoelectric coefficients in the hexagonal compounds. Likewise, the number and frequency of the Raman and infrared active modes change in monolayers compared to bulk (for the h and t compounds). With the reduced dimensionality of the materials, we find the dynamic charge of the system is nearly unchanged for the h and t compounds, but varies in magnitude and sign for the tc compounds, due to charge transfer and a change in the interlayer interaction.

Finally, our calculations of monolayer TcS_2 and $ReSe_2$ indicate that these monolayers of these materials will not be stable in the triclinic phase. When compared to our previous bulk calculations (Ref. [61]), it seems that stacking stabilizes the triclinic phase, indicating that the interlayer interaction plays an underappreciated role in these compounds. A determination of the low-temperature phase diagram and symmetry class of tc monolayers would be interesting but is beyond the scope of this work.

In conclusion, we have calculated the vibrational and dielectric properties of the most common transition metal dichalcogenides using the ABINIT software package, the DFT-D3 van der Waals functional, GGA exchange correlation, and norm-conserving pseudopotentials. Our calculations for the monolayer compounds are compared to bulk phases and experimental measurement, and show excellent agreement. We extract trends and outliers in the three symmetry classes. It is our hope that this information will stimulate experimental investigations of the less common TMD monolayers and serve to engineer heterostructures that combine the unique properties of the individual materials.

ACKNOWLEDGMENTS

The authors gratefully acknowledge funding from the Belgian Fonds National de la Recherche Scientifique FNRS under Grants No. PDR T.1077.15-1/7 (N.A.P. and M.J.V.), No. PDR T.0103.19 - ALPS (X.G. and M.J.V.), and an FRIA Grant (B.V.T.). N.A.P. would like to thank the Research Council of Norway through the Frinatek program for funding. M.J.V. and A.D. acknowledge support from ULg and from the Communauté Française de Belgique (Grant No. ARC AIMED 15/19-09). Computational resources have been provided by the Consortium des Equipements de Calcul Intensif en Fédération Wallonie Bruxelles (CECI), funded by FRS-FNRS Grant Agreement No. 2.5020.11; the Tier-1 supercomputer of the Fédération Wallonie-Bruxelles, funded by the Walloon Region under Grant Agreement No. 1117545; and by PRACE-

3IP DECI grants, on ARCHER and Salomon (ThermoSpin, ACEID, OPTOGEN, and INTERPHON 3IP Grant Agreement No. FP7 RI-312763 and 13 Grant Agreement No. 653838 of H2020).

[1] K. S. Novoselov, A. K. Geimand, S. V. Morozov, D. Jiang, Y. Zhang, S. V. Dubonos, I. V. Grigorieva, and A. A. Firsov, Science **306**, 666 (2004).
[2] A. Gupta, T. Sakthivel, and S. Seal, Prog. Mater. Sci. **73**, 44 (2015).
[3] S. Z. Butler, S. M. Hollen, L. Cao, Y. Chi, J. A. Gupta, H. R. Gutierrez, T. F. Heinz, S. S. Hong, J. Huang, A. F. Ismach, E. Johnston-Halperin, M. Kuno, V. V. Plashnitsa, R. D. Robinson, R. S. Ruoff, S. Salahuddin, J. Shan, L. Shi, M. G. Spencer, M. Terrones, W. Windl, and J. E. Goldberger, ACS Nano **7**, 2898 (2013).
[4] B. Dubertret, T. Heine, and M. Terrones, Acc. Chem. Res. **48**, 1 (2015).
[5] F. A. Rasmussen and K. S. Thygesen, J. Phys. Chem. C. **119**, 13169 (2015).
[6] R. Roldan, J. A. Silva-Guillen, M. P. Lopez-Sancho, F. Guinea, E. Cappelluti, and P. Ordejon, Ann. Phys. **526**, 347 (2014).
[7] A. Kuc, in *Chemical Modelling: Vol. 11*, edited by M. Springborg and J.-O. Joswig (The Royal Society of Chemistry, Cambridge, UK, 2015).
[8] D. Kireev and A. Offenhaeusser, 2D Mater. **5**, 042004 (2018).
[9] M. M. Alyoruk, Y. Aierken, D. Cakir, F. M. Peeters, and C. Sevik, J. Phys. Chem. C **119**, 23231 (2015).
[10] Q. H. Wang, K. Kalantar-Zadeh, A. Kis, J. N. Coleman, and M. S. Strano, Nat. Nanotechnol. **7**, 699 (2012).
[11] N. Huo, Z. Wei, X. Meng, J. Kang, F. Wu, S.-S. Li, S.-H. Wei, and J. Li, J. Mater. Chem. C **3**, 5467 (2015).
[12] D. Jariwala, V. K. Sangwan, L. J. Lauhon, T. J. Marks, and M. C. Hersam, ACS Nano. **8**, 1102 (2014).
[13] B. Radisavjevic, A. Radenovic, J. Brivio, V. Giacometti, and A. Kis, Nat. Nanotechnol. **6**, 147 (2011).
[14] J. M. Hamm and O. Hess, Science **340**, 1298 (2013).
[15] R. Zan, Q. M. Ramasse, R. Jalil, J.-S. Tu, U. Bangert, and K. S. Novoselov, J. Phys.: Conf. Ser. **902**, 012028 (2017).
[16] K. S. Novoselov, A. Mishchenko, A. Carvalho, and A. H. C. Neto, Science **353**, aac9439 (2016).
[17] J. S. Ross, P. Rivera, J. Schaibley, E. Lee-Wong, H. Yu, T. Taniguchi, K. Watanabe, J. Yan, D. Mandrus, D. Cobden, W. Yao, and X. Xu, Nano Lett. **17**, 638 (2017).
[18] R. M. Martin, *Electronic Structure: Basic Theory and Practice Methods* (Cambridge University Press, Cambridge, 2004).
[19] N. Mounet, M. Gibertini, P. Schwaller, A. Merkys, I. E. Castelli, A. Cepellotti, G. Pizzi, and N. Marzari, Nat. Nanotechnol. **13**, 246 (2018).
[20] K. Choudhary, I. Kalish, R. Beams, and F. Tavazza, Sci. Rep. **7**, 5179 (2017).
[21] S. Haastrup, M. Strange, M. Pandey, T. Deilmann, P. S. Schmidt, N. F. Hinsche, M. N. Gjerding, D. Torelli, P. M. Larsen, A. C. Riis-Jensen, J. Gath, K. W. Jacobsen, J. J. Mortensen, T. Olsen, and K. S. Thygesen, 2D Mater. **5**, 042002 (2018).
[22] X. Li, Z. Zhang, Y. Yao, and H. Zhang, 2D Mater. **5**, 045023 (2018).
[23] G. Petretto, S. Dwaraknath, H. P. C. Miranda, D. Winston, M. Giantomassi, M. J. van Setten, X. Gonze, K. A. Persson, G. Hautier, and G.-M. Rignanese, Sci. Data **5**, 180065 (2018).
[24] G. Petretto, X. Gonze, G. Hautier, and G.-M. Rignanese, Comput. Mater. Sci. **144**, 331 (2018).
[25] P. Chen, W. W. Pai, Y.-H. Chan, A. Takayama, C.-Z. Xu, A. Karn, S. Hasegawa, M. Y. Chou, S.-K. Mo, A.-V. Fedorov, and T.-C. Chiang, Nat. Commun. **8**, 516 (2017).
[26] D. J. Late, S. N. Shirodkar, U. V. Waghmare, V. P. Dravid, and C. N. R. Rao, ChemPhysChem **15**, 1592 (2014).
[27] I. G. Lezama, A. Arora, A. Ubaldini, C. Barreteau, E. Gianini, M. Potemski, and A. F. Morpurgo, Nano Lett. **15**, 2336 (2015).
[28] C. Ruppert, O. B. Aslan, and T. F. Heinz, Nano Lett. **14**, 6231 (2014).
[29] S. Tongay, H. Sahin, C. Ko, A. Luce, W. Fan, K. Liu, J. Zhou, Y.-S. Huang, C.-H. Ho, J. Yan, D. F. Ogletree, S. Aloni, J. Ji, S. Li, J. Li, F. M. Peeters, and J. Wu, Nat. Commun. **5**, 3252 (2014).
[30] Y. Feng, W. Zhou, Y. Wang, J. Zhou, E. Liu, Y. Fu, Z. Ni, X. Wu, H. Yuan, F. Miao, B. Wang, X. Wan, and D. Xing, Phys. Rev. B **92**, 054110 (2015).
[31] S. Manas-Valero, V. Garcia-Lopez, A. Cantarero, and M. Galbiati, Appl. Sci. **6**, 264 (2016).
[32] A. Molina-Sanchez and L. Wirtz, Phys. Rev. B **84**, 155413 (2011).
[33] A. Molina-Sanchez, K. Hummer, and L. Wirtz, Surf. Sci. Rep. **70**, 554 (2015).
[34] A. Kumar and P. K. Ahluwalia, MoS_2 *and Lecture Notes in Nanoscale Science and Technology* (Springer, New York, 2014), pp. 53–76.
[35] Q. Zhao, Y. Guo, K. Si, Z. Ren, J. Bai, and X. Xu, Phys. Stat. Sol. B **254**, 1700033 (2017).
[36] N. Glebko, I. Alaksandrova, G. C. Tewari, T. S. Tripathi, M. Karippinen, and A. J. Karttunen, J. Phys. Chem. C **122**, 26835 (2018).
[37] H. Guo, N. Lu, L. Wang, X.Wu, and X. C. Zeng, J. Phys. Chem. C **118**, 7242 (2014).
[38] E. M. Mannebach, C. Nyby, F. Ernst, Y. Zhou, J. Tolsma, Y. Li, M.-J. Sher, I.-C. Tung, H. Zhou, Q. Zhang, K. L. Seyler, G. Clark, Y. Lin, D. Zhu, J. M. Glownia, M. E. Kozina, S. Song, S. Nelson, A. Mehta, Y. Yu, A. Pant, O. B. Aslan, A. Raja, Y. Guo, A. DiChiara, W. Mao, L. Cao, S. Tongay, J. Sun, D. J. Singh, T. F. Heinz, X. Xu, A. H. MacDonald, E. Reed, H. Wen, and A. M. Lindenberg, Nano Lett. **17**, 7761 (2017).
[39] D. Straub, M. Skibowski, F. J. Himpsel, and W. Drube, Phys. Rev. B **31**, 8254 (1985).
[40] C. Yuan, F. Valla, F. Shiang, W. Kenji, T. Takashi, K. Efthimios, and J.-H. Pablo, Nature (London) **556**, 43 (2018).
[41] S. Moriyam, Y. Morita, K. Komatsu, K. Endo, T. Iwasaki, S. Nakaharai, Y. Noguchi, Y. Wakayama, E. Watanabe, D. Tsuya, K. Watanabe, and T. Taniguchi, arXiv:1901.09356.

[42] C. Chiritescu, D. G. Cahill, N. Nguyen, D. Johnson, A. Bodapati, P. Keblinski, and P. Zshack, Science **315**, 351 (2007).

[43] C. Woods, L. Britnell, A. Eckmann, R. Ma, J. Lu, H. Guo, X. Lin, G. Yu, Y. Cao, R. Gorbachev, A. Kretinin, J. Park, L. Ponomarenko, M. Katsnelson, Y. Gornostyrev, K. Watanabe, T. Taniguchi, C. Casiraghi, H.-J. Gao, A. Geim, and K. Novoselov, Nat. Phys. **10**, 451 (2014).

[44] C. Espejo, T. Rangel, A. H. Romero, X. Gonze, and G.-M. Rignanese, Phys. Rev. B **87**, 245114 (2013).

[45] H. Lim, S. I. Yoon, G. Kim, A.-R. Jang, and H. Shin, Chem. Mater. **26**, 4891 (2014).

[46] A. F. Rigosi, H. M. Hill, A. Chernikov, and T. F. Heinz, Nano Lett. **15**, 5033 (2015).

[47] N. R. Wilson, P. V. Nguyen, K. Seyler, P. Rivera, A. J. Marsden, Z. P. L. Laker, G. C. Constantinescu, V. Kandyba, A. Barinov, N. D. M. Hine, X. Xu, and D. H. Cobden, Science **3**, 1601832 (2017).

[48] B. VanTroeye, A. Lherbier, J.-C. Charlier, and X. Gonze, Phys. Rev. Mater. **2**, 074001 (2018).

[49] C. Zhang, C.-P. Chuu, X. Ren, M.-Y. Li, L.-J. Li, C. Jin, M.-Y. Chou, and C.-K. Shih, Sci. Adv. **3**, e1601459 (2017).

[50] Z. Xin, T. Qing-Hai, W. Jiang-Bin, S. Wei, and T. Ping-Heng, Nanoscale **8**, 6435 (2016).

[51] E. del Corro, A. Botello-Méndez, Y. Gillet, A. L. Elias, H. Terrones, S. Feng, C. Fantini, D. Rhodes, N. Pradhan, L. Balicas, X. Gonze, J.-C. Charlier, M. Terrones, and M. A. Pimenta, Nano Lett. **16**, 2363 (2016).

[52] R. Zhang and R. Cheung, *Two-dimensional Materials* (InteChOpen, London, UK, 2016), Chap. 10.

[53] See Supplemental Material at http://link.aps.org/supplemental/10.1103/PhysRevMaterials.3.074009 which includes Refs. [5,11,19,21,28,29,35–37,72,75,76,78–82,84,89–98,100,104,110,111,113–115,131,134,143,144] and numerical data on the remainder of the compounds considered here.

[54] X. Gonze, Phys. Rev. B **55**, 10337 (1997).

[55] S. Baroni, S. de Gironcoli, A. D. Corso, and P. Giannozzi, Rev. Mod. Phys. **73**, 515 (2001).

[56] X. Gonze and C. Lee, Phys. Rev. B **55**, 10355 (1997).

[57] M. J. Verstraete and Z. Zanolli, in *Computing Solids: Models and Ab-initio Methods and Supercomputing, Lecture Notes of the 45th Spring School 2014*, edited by S. Blügel, N. Helbig, V. Meden, and D. Wortmann (Schiften des Forschungszentrums Julich, Germany, 2014).

[58] X. Gonze, G.-M. Rignanese, M. Verstraete, J.-M. Beuken, Y. Pouillon, R. Caracas, F. Jollet, M. Torrent, G. Zerah, M. Mikami, P. Ghosez, M. Veithen, J.-Y. Raty, V. Olevano, F. Bruneval, L. Reining, R. Godby, G. Onida, D. Hamann, and D. Allan, Z. Kristallogr. **220**, 558 (2005).

[59] X. Gonze, B. Amadon, P. M. Anglade, J.-M. Beuken, F. Bottin, P. Boulanger, F. Bruneval, D. Caliste, R. Caracas, M. Cote, T. Deutsch, L. Genovese, P. Ghosez, M. Giantomassi, S. Goedecker, D. Hamann, P. Hermet, F. Jollet, G. Jomard, S. Leroux, M. Mancini, S. Mazevet, M. Oliveira, G. Onida, Y. Pouillon, T. Rangel, G.-M. Rignanese, D. Sangalli, R. Shaltaf, M. Torrent, M. Verstraete, G. Zerah, and J. Zwanziger, Comput. Phys. Commun. **180**, 2582 (2009).

[60] X. Gonze, F. Jollet, F. A. Araujo, D. Adams, B. Amadon, T. Applencourt, C. Audouze, J.-M. Beuken, J. Bieder, A. Bokhanchuk, E. Bousquet, F. Bruneval, D. Caliste, M. Cote, F. Dahm, F. D. Pieve, M. Delaveau, M. D. Gennaro, B. Dorado, C. Espejo, G. Geneste, L. Genovese, A. Gerossier, M. Giantomassi, Y. Gillet, D. Hamann, L. He, G. Jomard, J. L. Janssen, S. L. Roux, A. Levitt, A. Lherbier, F. Liu, I. Lukacevic, A. Martin, C. Martins, M. Oliveira, S. Ponce, Y. Pouillon, T. Rangel, G.-M. Rignanese, A. Romero, B. Rousseau, O. Rubel, A. Shukri, M. Stankovski, M. Torrent, M. VanSetten, B. V. Troeye, M. Verstraete, D. Waroquiers, J. Wiktor, B. Xu, A. Zhou, and J. W. Zwanziger, Comput. Phys. Commun. **205**, 106 (2016).

[61] N. A. Pike, A. Dewandre, B. Van Troeye, X. Gonze, and M. J. Verstraete, Phys. Rev. Mater. **2**, 063608 (2018).

[62] J. P. Perdew, K. Burke, and M. Ernzerhof, Phys. Rev. Lett. **77**, 3865 (1996).

[63] M. Fuchs and M. Scheffler, Comput. Phys. Commun. **119**, 67 (1999).

[64] E. J. Walter and A. Rappe, OPIUM pseudopotential package, http://opium.sourceforge.net/ (April 2018).

[65] D. R. Hamann, Phys. Rev. B **88**, 085117 (2013).

[66] S. Grimme, S. Ehrlich, and L. Goerigk, J. Chem. Phys. **132**, 154104 (2010).

[67] B. Van Troeye, M. Torrent, and X. Gonze, Phys. Rev. B **93**, 144304 (2016).

[68] B. Van Troeye, M. J. van Setten, M. Giantomassi, M. Torrent, G.-M. Rignanese, and X. Gonze, Phys. Rev. B **95**, 024112 (2017).

[69] H. J. Monkhorst and J. D. Pack, Phys. Rev. B **13**, 5188 (1976).

[70] M. Veithen, X. Gonze, and P. Ghosez, Phys. Rev. B **71**, 125107 (2005).

[71] D. M. Ceperley and B. J. Alder, Phys. Rev. Lett. **45**, 566 (1980).

[72] H. Zeng, G.-B. Liu, J. Dai, Y. Yan, B. Zhu, R. He, L. Xie, S. Xu, X. Chen, W. Yao, and X. Cui, Sci. Rep. **3**, 1608 (2013).

[73] D. Wolverson and L. S. Hart, Nanoscale Res. Lett. **11**, 250 (2016).

[74] R. Caracas and R. E. Cohen, Geophys. Res. Lett. **33**, L12S05 (2006).

[75] P. Joensen, E. D. Crozier, A. Alberding, and R. F. Frindt, J. Phys. C: Sol. State **20**, 4043 (1987).

[76] X. Wang, L. Haung, X.-W. Jiang, Y. Li, Z. Wei, and J. Li, J. Mat. Chem. C **4**, 3143 (2016).

[77] M. Gehlmann, I. Aguilera, G. Bihlmayer, S. Nemsak, P. Nagler, P. Gospodaric, G. Zamborlini, M. Eschbach, V. Feyer, F. Kronast, E. Mlynczak, T. Korn, L. Plucinski, C. Schuller, S. Blugel, and C. M. Schneider, Nano Lett. **17**, 5187 (2017).

[78] K. Liu, Q. Yan, M. Chen, W. Fan, Y. Sun, J. Suh, D. Fu, S. Lee, J. Zhou, S. Tongay, J. Ji, J. B. Neaton, and J. Wu, Nano Lett. **14**, 5097 (2014).

[79] J. Kang, S. Tongay, J. Zhou, J. Lo, and J. Wu, Appl. Phys. Lett. **102**, 012111 (2013).

[80] Q. Zhao, Y. Guo, Y. Zhou, X. Xu, Z. Ren, J. Bai, and X. Xu, J. Phys. Chem. C **121**, 23744 (2017).

[81] G. Casillas, U. Santiago, H. Barrón, D. Alducin, A. Ponce, and M. José-Yacamán, J. Phys. Chem. **119**, 710 (2015).

[82] T. Sohier, M. Calandra, and F. Mauri, Phys. Rev. B **96**, 159904(E) (2017).

[83] H. Zhu, W. Wang, J. Xiao, M. Liu, S. Xiong, Z. J. Wong, Z. Ye, Y. Ye, Z. Yin, and X. Zhang, Nat. Nano **10**, 151 (2015).

[84] R. I. Woodward, R. T. Murray, C. F. Phelan, R. E. P. de Oliveire, T. H. Runcorn, E. J. R. Kellehel, S. Li, E. C. de Oliveira, G. J. M. Fechine, G. Eda, and C. J. S. de Matos, 2d Mater. **4**, 011006 (2017).

[85] L. S. Hart, J. L. Webb, S. Dale, S. J. Bending, M. Mucha-Kruczynski, D. Wolverson, C. Chen, J. Avila, and M. C. Asensio, Sci. Rep. **7**, 5145 (2017).

[86] J. L. Webb, L. S. Hart, D. Wolverson, C. Chen, J. Avila, and M. C. Asensio, Phys. Rev. B **96**, 115205 (2017).

[87] L. Lindsay and D. A. Broido, Phys. Rev. B **81**, 205441 (2010).

[88] L. F. C. Pereira and D. Donadio, Phys. Rev. B **87**, 125424 (2013).

[89] T. Boker, R. Severin, A. Muller, C. Janowitz, R. Manzke, D. Voß, P. Kruger, A. Mazur, and J. Pollmann, Phys. Rev. B **64**, 235305 (2001).

[90] Y.-H. Chang, W. Zhang, Y. Zhu, Y. Han, J. Pu, J.-K. Chang, W.-T. Hsu, J.-K. Huang, C.-L. Hsu, M.-H. Chiu, T. Takenobu, H. Li, C.-I. Wu, W.-H. Chang, A. T. S. Wee, and L.-J. Li, ACS Nano **8**, 8582 (2014).

[91] A. Berkdemir, H. R. Guiterrez, A. R. Botello-Mendez, N. Perea-Lopez, A. L. Elias, C.-I. Chia, V. H. Crespi, F. Lopez-Urias, J.-C. Charlier, H. Terrones, and M. Terrones, Sci. Rep. **3**, 1755 (2013).

[92] C.-Y. Wang and G. Guo, J. Phys. Chem. C **119**, 13268 (2015).

[93] Y. Han, S. Xie, B. Savitzky, R. Hovdan, H. Gao, L. F. Kourkoutis, J. Park, and D. A. Muller, Microsc. Microanal. **22**, 870 (2016).

[94] Z. Zeng, Z. Yin, X. Huang, H. Li, Q. He, G. Lu, F. Boey, and H. Zhang, Agnew. Chem. Int. Ed. Engl. **50**, 11093 (2011).

[95] P. Chen, Y.-H. Chan, X.-Y. Fang, Y. Zhang, M. Y. Chou, S.-K. Mo, Z. Hussain, A. V. Fedorov, and T. C. Chaing, Nat. Commun. **6**, 8943 (2015).

[96] J.-P. Peng, J. Q. Guan, H.-M. Zhang, C.-L. Song, L. Wang, K. He, Q. K. Xue, and X. C. Ma, Phys. Rev. B **91**, 121113(R) (2015).

[97] M. J. Mleczko, C. Zhang, H. R. Lee, H.-H. Kuo, B. Magyari-Köpe, R. G. Moore, Z.-X. Shen, I. R. Fisher, Y. Nishi, and E. Pop, Science Advances **3**, e1700481 (2017).

[98] S. Jiang, M. Hong, W. Wei, L. Zhao, N. Zhang, Z. Zhang, P. Yang, N. Gao, X. Zhou, C. Xie, J. Shi, Y. Huan, L. Tong, J. Zhao, Q. Zhang, Q. Fu, and Y. Zhang, Commun. Chem. **1**, 17 (2018).

[99] H. Zhao, J. Wu, H. Zhong, Q. Guo, X. Wang, F. Xia, L. Yang, P. Tan, and H. Wang, Nano Res. **8**, 3651 (2015).

[100] J. F. Nye, *Physical Properties of Crystals* (Oxford University Press, London, 1957).

[101] N. W. Tschoegl, Aus. J. Phys. **11**, 154 (1957).

[102] P. Dłużewski, T. D. Young, G. P. Dimitrakopulos, J. Kioseoglou, and P. Komninou, *Nonlinear Finite Element and Atomistic Modeling of Dislocations in Heterostructures* (Springer, Berlin, 2010).

[103] D. Tromans, Int. J. Res. Rev. Appl. Sci. **6**, 462 (2011).

[104] R. Zhang, V. Koutes, and R. Cheung, Appl. Phys. Lett. **108**, 042104 (2016).

[105] S. Dai, Y. Xiang, and D. J. Srolovitz, Nano Lett. **16**, 5923 (2016).

[106] A. E. H. Love, Philos. Trans. R. Soc., A **179**, 491 (1888).

[107] K. Lai, W.-B. Zhang, F. Zhou, F. Zeng, and B.-Y. Tang, J. Phys. D: Appl. Phys. **49**, 185301 (2016).

[108] N. Lindahl, D. Midtvedt, J. Svensson, O. A. Nerushev, N. Lindvall, A. Isacsson, and E. E. B. Campbell, Nano Lett. **12**, 3526 (2012).

[109] R. Nicklow, N. Wakabayashi, and H. G. Smith, Phys. Rev. B **5**, 12 (1974).

[110] C. Sevik, A. U. J. Sci. and Tech. A **18**, 632 (2017).

[111] N. Scheuschner, R. Gillen, M. Staiger, and J. Maultzsch, Phys. Rev. B **91**, 235409 (2015).

[112] W. Setyawan and S. Curtarolo, Comptut. Mater. Sci. **49**, 299 (2010).

[113] W.-T. Hsu, L.-S. Lu, D. Wang, J.-K. Huang, M-Y-Li, T.-R. Chang, Y.-C. Chou, Z.-Y. Juang, H.-Y. Jeng, L.-J. Li, and W.-H. Chang, Nat. Commun. **8**, 1 (2017).

[114] Y. Zhang, T.-R. Chang, B. Zhou, Y.-T. Cui, H. Yan, Z. Liu, F. Schmitt, J. Lee, R. Moore, Y. Chen, H. Lin, H.-Y. Jeng, S.-K. Mo, Z. Hussain, A. Bansil, and Z.-X. Shen, Nat. Nano **9**, 111 (2014).

[115] J. Lu, A. Carvalho, X. K. Chan, H. Liu, B. Liu, E. S. Tok, K. P. Loh, A. H. C. Neto, and C. H. Sow, Nano Lett. **15**, 3524 (2015).

[116] H. M. Hill, A. F. Rigosi, C. Roquelet, A. Chernikov, T. C. Berkelbach, D. R. Reichman, M. S. Hybertsen, L. E. Brus, and T. F. Heinz, Nano Lett. **15**, 2992 (2015).

[117] N. Saigal, V. Sugunakar, and S. Ghosh, Appl. Phys. Lett. **108**, 132105 (2016).

[118] A. F. Rigosi, H. M. Hill, K. T. Rim, G. W. Flynn, and T. F. Heinz, Phys. Rev. B **94**, 075440 (2016).

[119] A. T. Handbicki, M. Currie, G. Kioselglou, A. L. Friedman, and B. T. Jonker, Solid State Commun. **203**, 16 (2015).

[120] I. Kylanpaa and H.-P. Komsa, Phys. Rev. B **92**, 205418 (2015).

[121] M. M. Ugeda, A. J. Bradley, S.-F. Shi, F. H. da Jornada, Y. Zhang, D. Y. Qiu, W. Ruan, S.-K. Mo, Z. Hussain, Z.-X. Shen, F. Wang, S. G. Louie, and M. F. Crommie, Nat. Mater. **13**, 1091 (2014).

[122] F. Aryasetiawan and O. Gunnarsson, Rep. Prog. Phys. **61**, 237 (1998).

[123] J. P. Perdew, Int. J. Quantum Chem. **28**, 497 (1985).

[124] A. Kormanyos, G. Burkard, M. Gmitra, J. Fabian, V. Zolyomi, N. D. Drummond, and V. Fal'ko, 2D Mater. **2**, 022001 (2015).

[125] Y. Wang, C. Cong, W. Yang, J. Shang, N. Peimyoo, Y. Chen, J. Kang, J. Wang, W. Huang, and T. Yu, Nano Res. **8**, 2562 (2015).

[126] J. Kang, L. Zhang, and S.-H. Wei, J. Phys. Chem. Lett. **7**, 597 (2016).

[127] W. Czaja and I. Gränacher, Helv. Phys. Acta **36**, 1073 (1963).

[128] N. A. Pike, B. VanTroeye, A. Dewandre, G. Petretto, X. Gonze, G. M. Rignanese, and M. J. Verstraete, Phys. Rev. B **95**, 201106(R) (2017).

[129] T. Sohier, M. Calandra, and F. Mauri, Phys. Rev. B **94**, 085415 (2016).

[130] M. Danovich, I. L. Aleiner, N. D. Drummond, and V. I. Fal'ko, IEEE J. Sel. Top. Quantum Electron. **23**, 6000105 (2017).

[131] K. L. Seyler, J. R. Schaibley, P. Gong, P. Rivera, A. M. Jones, S. Wu, J. Yan, D. G. Mandrus, W. Yao, and X. Xu, Nat. Nanotechnol. **10**, 407 (2015).

[132] H. Wang and X. Qian, Nano Lett. **17**, 5027 (2017).

[133] N. Kumar, S. Najmaei, Q. Cui, F. Ceballos, P. M. Ajayan, J. Lou, and H. Zhao, Phys. Rev. B **87**, 161403(R) (2013).

[134] Z. Zhao, H. Zhang, H. Yuan, S. Wang, Y. Lin, Q. Zeng, G. Xu, Z. Liu, G. K. Solanki, K. D. Patel, Y. Chi, H. Y. Hwang, and W. L. Mao, Nat. Commun. **6**, 7312 (2015).
[135] P. L. de Andres, F. Guinea, and M. I. Katsnelson, Phys. Rev. B **86**, 144103 (2012).
[136] T. Sohier, M. Gibertini, M. Calandra, F. Mauri, and N. Marzari, Nano Lett. **17**, 3758 (2017).
[137] T. Sohier, M. Calandra, and F. Mauri, Phys. Rev. B **96**, 075448 (2017).
[138] W. Kohn, Phys. Rev. Lett. **2**, 393 (1959).
[139] C. Ataca, H. Sahin, and S. Ciraci, J. Phys. Chem. C **116**, 8983 (2012).
[140] K. Dolui and S. Sanvito, E. Phys. Lett. **115**, 47001 (2016).
[141] K. Sugawara, Y. Nakata, R. Shimizu, P. Han, T. Hitosugi, T. Sato, and T. Takahashi, ACS Nano. **10**, 1341 (2016).
[142] D. L. Duong, M. Burghard, and J. C. Schon, Phys. Rev. B **92**, 245131 (2015).
[143] Y. Jiao, L. Zhou, F. Ma, G. Gao, L. Kou, J. Bell, S. Sanvito, and A. Du, ACS Appl. Mater. Interfaces **8**, 5385 (2016).
[144] X. Zhu, Y. Cao, J. Zhang, E. W. Plummer, and J. Guo, Proc. Natl. Acad. Sci. USA **112**, 2367 (2015).